Three-Dimensional Imaging of Lamina Cribrosa Defects in Glaucoma Using Swept-Source Optical Coherence Tomography

Kohei Takayama,[1] Masanori Hangai,[1] Yugo Kimura,[1] Satoshi Morooka,[1] Masayuki Nukada,[1] Tadamichi Akagi,[1] Hanako Ohashi Ikeda,[1] Akiko Matsumoto,[1,2] and Nagahisa Yoshimura[1]

[1]Department of Ophthalmology and Visual Sciences, Kyoto University Graduate School of Medicine, Kyoto, Japan
[2]Topcon Corporation, Tokyo, Japan

Correspondence: Masanori Hangai, Department of Ophthalmology and Visual Sciences, Kyoto University Graduate School of Medicine, 54 Kawahara-cho, Shogoin, Sakyo-ku, Kyoto 606-8507, Japan; hangai@kuhp.kyoto-u.ac.jp.

Submitted: January 17, 2013
Accepted: June 9, 2013

Citation: Takayama K, Hangai M, Kimura Y, et al. Three-dimensional imaging of lamina cribrosa defects in glaucoma using swept-source optical coherence tomography. *Invest Ophthalmol Vis Sci*. 2013;54:4798–4807. DOI:10.1167/iovs.13-11677

Purpose. To visualize lamina cribrosa defects using three-dimensional (3D) swept-source optical coherence tomography (SS-OCT), and to determine the factors associated with this feature.

Methods. All subjects were examined using an SS-OCT prototype system, which uses a tunable laser as a light source, operated at 100,000 Hz A-scan repetition rate in the 1050-nm wavelength. A 3D raster scan protocol consisting of 256 × 256 A-scans was acquired over a square area of 3 mm × 3 mm centered on the optic disc. En face sectioned volume and serial en face images and orthogonal (horizontal and vertical) serial B-scans were evaluated.

Results. A total of 182 eyes of 111 patients with glaucoma and 29 healthy eyes of 26 subjects were included. Twenty full-thickness focal lamina cribrosa defects were found in 12 (6.6%) of 182 eyes with glaucoma, whereas no lamina defects were found in healthy eyes. Nine eyes (75.0%) showed 15 full-thickness lamina cribrosa defects near the margin of the lamina cribrosa, and 3 eyes showed 4 lamina defects at the margin, as if detached from the sclera. Focal lamina cribrosa defects corresponded with neuroretinal rim thinning, concurrent or previous disc hemorrhages, abnormal circumpapillary retinal nerve fiber layer thickness, and visual field defects. The presence of lamina cribrosa defects was significantly associated with longer axial length and disc hemorrhages ($P = 0.033$ and 0.024, respectively).

Conclusions. 3D SS-OCT imaging allows visualization of the lamina cribrosa defects, which may be more prevalent in eyes with longer axial length and related to disc hemorrhages.

Keywords: glaucoma, lamina cribrosa, optical coherence tomography

Lamina cribrosa has been implicated as the principal site of damages to retinal ganglion cell (RGC) axons in glaucoma.[1–5] Lamina cribrosa is thought to be the supporting structure for unmyelinated RGC axons that make a 90° turn. It has a three-dimensional (3D) meshwork structure consisting of capillaries,, fenestrated sheets of scleral collagenous tissue, and occasional elastic fibers. Astrocytes separate the sheets and line the fenestrae, and the fascicles of RGC axons leave the eye through these openings (called pores).[6–8]

Earlier histopathological studies using animal, cadaver, or enucleated eyes showed morphological changes of the whole structure of the lamina cribrosa associated with glaucoma, such as thinning and U- or W-shaped posterior lamina displacement.[2,3,5] Increased intraocular pressure (IOP) or a translaminar pressure gradient is thought to cause these bulk changes in lamina cribrosa.[5,9–12] These deformations of the lamina cribrosa lead to misalignment of the connective tissue constituting the fenestrae, which then leads to compression, extension, and shearing of RGC axons or laminar capillaries within the lamina cribrosa, which result in the loss of RGCs.[9–11]

Recent advancement in imaging modalities provide a unique opportunity to observe lamina cribrosa structures in vivo. Spectral domain optical coherence tomography (SD-OCT) allows 3D imaging of the lamina cribrosa and laminar pores.[13–16] 3D SD-OCT imaging demonstrated thinning and posterior displacement of the lamina cribrosa, consistent with earlier histopathological findings.[14,16] SD-OCT technology also allows enhanced depth imaging (EDI), which improves visualization of the deep fundus structures including the lamina cribrosa.[17–19] Recently, the EDI-OCT method was successfully used in the discovery of a local abnormality of lamina cribrosa, termed focal lamina cribrosa defect, which was associated with local glaucomatous optic disc changes such as neuroretinal rim thinning/notching or acquired pits of the optic nerve (APONs).[20,21] This interesting feature has not been reported in the earlier histopathological articles on glaucomatous eyes.

Swept-source OCT (SS-OCT) with a 1050-nm tunable laser is the next generation of OCT technology, which allows 3D high-penetration imaging of the deep fundus tissue, such as the choroid and lamina cribrosa.[22–25] SS-OCT allows 3D raster scan with ideal sampling density, which enables clear observation of 3D structure of the optic disc including lamina cribrosa,[25] because this technology does not require averaging many B-scans to visualize the deep tissue.[23] Observation of the 3D optic disc dataset in arbitrary serial sections, such as en face scans (C-scan) and vertical and horizontal B-scans, and comparison of the en face images with optic disc photographs would be instrumental in for determining actual lamina cribrosa defects

Copyright 2013 The Association for Research in Vision and Ophthalmology, Inc.

Downloaded From: https://iovs.arvojournals.org/pdfaccess.ashx?url=/data/journals/iovs/932985/ on 11/11/2018

by excluding vascular shadowing-related artifacts. The purpose of the current study was to identify focal lamina cribrosa defects by using our prototype 3D SS-OCT system.[23,24] The second purpose was to determine the clinical factors associated with the focal lamina cribrosa defects identified with 3D SS-OCT imaging.

Methods

Candidates in this prospective study were glaucoma patients and healthy subjects who visited Kyoto University Hospital (Kyoto, Japan) and agreed to participate in this study between July 7, 2010, and January 6, 2012. All investigations in this study adhered to the tenets of the Declaration of Helsinki, and the study was approved by the Institutional Review Board and Ethics Committee of Kyoto University Graduate School of Medicine. Written informed consent was obtained from all subjects.

All participants underwent a comprehensive ophthalmic examination that included uncorrected and best-corrected visual acuity using the 5-m Landolt chart, slit-lamp biomicroscopy, Goldmann applanation tonometry, gonioscopy; measurements of axial length using IOLMaster (Carl Zeiss-Meditec, Dublin, CA), Heidelberg Retina Tomograph II (HRA2; Heidelberg Engineering, Heidelberg, Germany); achromatic automated perimetry using the 24-2 Swedish interactive threshold algorithm standard program (Humphrey Visual Field Analyzer II; Carl Zeiss-Meditec); dilated stereoscopic examination of optic disc and fundus, stereo disc photography with a 3-Dx simultaneous stereo disc camera (Nidek, Gamagori, Japan); and Spectralis HRA+OCT (Heidelberg Engineering). All patients underwent evaluation of the optic disc, including disc hemorrhages, at every 3-month visit to our clinic from the initial visit. Whenever the disc hemorrhage was found, the fundus photograph was taken.

To be included, eyes had to have best-corrected visual acuity of $\geq$20/40, spherical refraction within $\pm$6.0 diopters, cylinder correction within $\pm$3.0 diopters, and reliable visual field tests. Exclusion criteria were evidence of media opacities, such as corneal opacity, cataract, and vitreous opacity; vitreoretinal disease, uveitis, or nonglaucomatous optic neuropathy; or a history of intraocular surgery. Those patients with intraocular disease (e.g., diabetic retinopathy or retinal vein occlusion) or systemic (uncontrolled hypertension) or neurologic disease (e.g., pituitary tumor, cerebral infarction) that could affect the optic nerve structure or visual function were also excluded from this study.

Healthy eyes had to have IOP between 10 and 21 mm Hg, a normal open anterior chamber angle, clinically normal appearance of the optic disc, and normal visual field results. Glaucoma was defined as having glaucomatous appearance of the optic disc (localized or diffuse neuroretinal rim thinning or retinal nerve fiber layer defects) associated with typically glaucomatous, reproducible visual field defects on standard automated perimetry. Visual field results were considered reliable based on fixation loss $\leq$15%, false positive $\leq$15%, and false negative $\leq$15%. Anderson-Patella criteria was used to define glaucomatous visual field results on standard automated perimetry: glaucoma hemifield test outside normal limits, pattern standard deviation probability $<$5%, or a cluster of three or more adjacent nonedge points in typically glaucomatous locations that did not cross the horizontal meridian, all of which were depressed on the pattern deviation plot at a P value of $<$5% and one of which was depressed at a P value of $<$1%, confirmed with two reliable consecutive tests.

3D SS-OCT at 1050 nm

A prototype SS-OCT system with an axial scan rate of 100,000 Hz was fabricated for patient examination at Kyoto University Hospital, Japan, by Topcon Corporation (Tokyo, Japan).[23,24] This prototype SS-OCT used a wavelength-sweeping laser (tunable laser) with a tuning range of $\sim$199 nm centered at 1050 nm, yielding 8 μm axial resolution in tissue. Transverse resolution was set to $\sim$20 μm. SS-OCT imaging at 1050 nm was conducted with light intensity of $\sim$1 mW on the cornea, which is well below the safe retinal exposure limit established by the American National Standards Institute. Sensitivity was measured at $\sim$98 dB at this input power.

A 3D raster scan protocol consisting of 256 $\times$ 256 A-scans was acquired in 0.8 seconds over a square area of 3 mm $\times$ 3 mm, centered on the optic disc center. Volume rendering was performed in order to generate en face 3D images from the 3D data set. En face sectioned volume images and serial en face images were reconstructed for the 3D data set. These en face images and vertical and horizontal serial B-scan images were used to observe the laminar structures.

Assessment of Lamina Cribrosa Defects

The 3D OCT image set that was obtained was independently reviewed for focal defects of the lamina cribrosa by two graders (KT and YK), who were masked to all other information. A focal full-thickness lamina cribrosa defect was defined as the loss of high reflectivity from the anterior-to-posterior border of the lamina cribrosa on vertical/horizontal serial B-scan images and a maximum width of hyporeflectivity on en face images of $>$100 μm.[28] The anterior and posterior borders of the lamina cribrosa on B-scans were defined as the locations where high reflectivity started and ended beneath the optic disc cup, respectively. In addition, the observers confirmed that the candidate lamina cribrosa defects did not correspond to hyporeflectivity due to vascular shadowing by comparing the en face images to the disc photograph (Figs. 1, 2). When a full-thickness loss of the high lamina reflectivity corresponded to the hyporeflective vascular pattern on the en face images corresponding to the retinal blood vessels on disc photographs, it was not included (Fig. 1). Conversely, a hyporeflective spot on the en face images that could not be recognized as full-thickness loss of the lamina reflectivity on B-scan images was not included as a full-thickness lamina cribrosa defect. If the two graders did not agree on the existence of the lamina cribrosa defect, they reviewed and discussed the lamina cribrosa until a consensus was reached. If no consensus could be reached, the candidate lamina cribrosa defect was excluded from analysis.

We compared the angular location of the lamina cribrosa defects on en face images and the glaucomatous features, such as neuroretinal rim thinning, localized retinal nerve fiber layer (RNFL) defects, and disc hemorrhages, on color disc photographs. The angle of the edges of each lesion centered on the optic disc center was measured using Screen Protractor version 1.1 software for Windows Screen Protractor version 1.1 software (Softonic, http://screen-protractor.en.softonic.com/) for Windows (Microsoft Corporation, Redmond, WA). When the angular location of a lamina cribrosa defect overlapped with that of each photographic glaucomatous feature, we concluded that the lamina cribrosa defect spatially corresponded with the photographic feature.

Statistical Analysis

Statistical analysis was performed using SPSS Statistics version 20 software (IBM, New York, NY). The continuous data were

Investigative Ophthalmology & Visual Science

Downloaded From: https://iovs.arvojournals.org/pdfaccess.ashx?url=/data/journals/iovs/932985/ on 11/11/2018

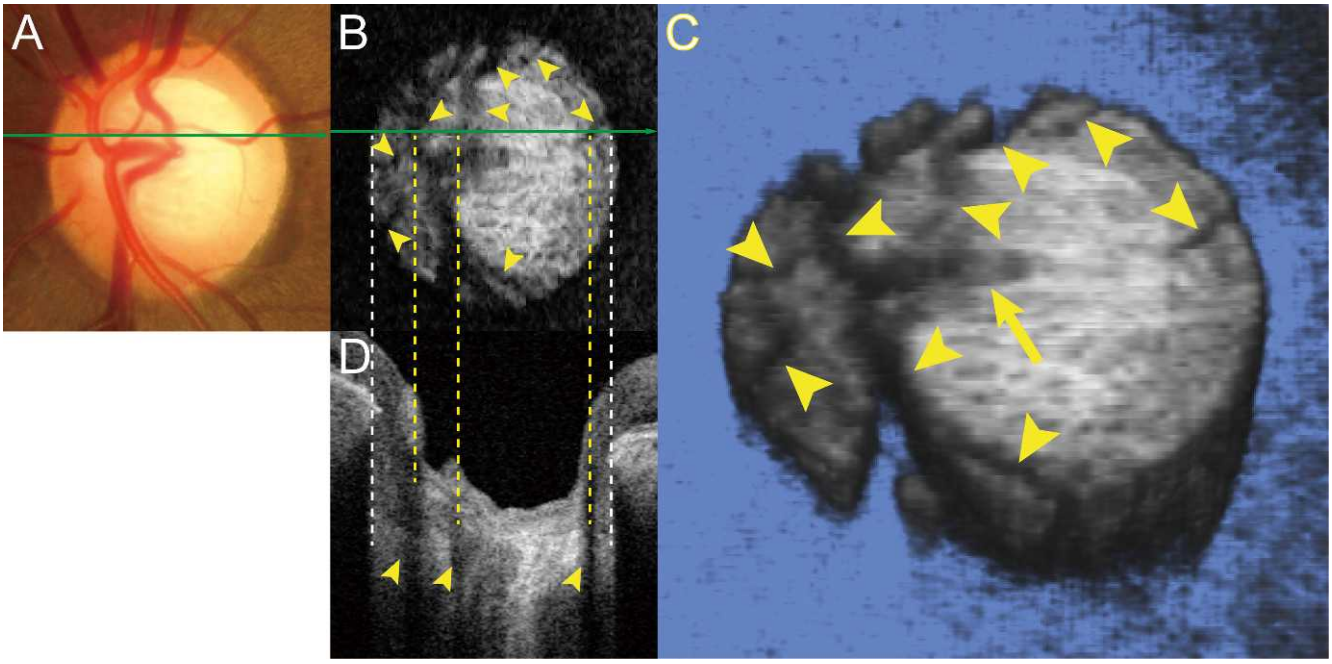

FIGURE 1. 3D imaging of the lamina cribrosa with 1-μm SS-OCT at 1050 nm in a healthy eye. (**A**) Color disc photograph. (**B**) En face image of the optic disc at the level of the lamina cribrosa reconstructed from a 3D SS-OCT data set. A comparison between the disc photograph and the en face image revealed that the hyporeflective pattern (*yellow arrowheads*) accurately corresponded to the retinal blood vessels on the optic disc. The hyporeflective regions do not represent lamina cribrosa defects but are artifactual features that resulted from signal blocking by the retinal blood vessels (termed vascular shadowing). (**C**) En face volume image sectioned at the level of the lamina cribrosa reconstructed from the 3D SS-OCT data set. Artifactual defects (*yellow arrowheads*) are shown on the highly reflective lamina cribrosa, caused by the vascular shadowing. (**D**) Horizontal B-scan along the *green line* (**A**, **B**). Lamina cribrosa reflectivity appears to have defects (*yellow arrowheads*), but these defects correspond to hyporeflective vascular regions ([**B**], *yellow dotted line*), thus indicating that these are artifacts and not lamina cribrosa defects. Vascular shadowing is characterized by the axially straight hyporeflectivity throughout the area beneath the blood vessels.

compared between eyes with and without lamina cribrosa defects by using Mann-Whitney *U* test. Cohen's κ coefficient was used to estimate inter-rater reliability for identifying lamina cribrosa defects. The categorical data were compared between groups using the χ^2 test. To determine the effects of various factors on the presence of focal lamina cribrosa defects, we performed univariate and multivariate logistic regression analyses. A *P* value of <0.05 was considered statistically significant.

RESULTS

A total of 182 glaucomatous eyes of 111 Japanese patients (50 men, 62 women) were eligible for the current study. Patients ranged in age from 21 to 89 years old (mean ± SD, 62.9 ± 14.4 years). Glaucomatous eyes ranged in spherical equivalents of refractive errors from –6.0 to 3.0 (–1.65 ± 2.30 diopters [D]), in axial length from 21.44 to 27.9 mm (mean ± SD, 24.5 ± 1.29 mm), and in visual field mean deviation (MD) from –31.29 to 0.63 dB (–10.9 ± 9.29 dB). Our glaucomatous eyes included 62 eyes (44 patients) with high-tension open-angle glaucoma (HTG; known untreated IOP > 21 mm Hg, twice), 104 eyes (69 patients) with normal-tension open-angle glaucoma (NTG; untreated IOP ≤ 21 mm Hg, at all times), and 16 eyes (12 patients) with secondary glaucoma (exfoliation glaucoma, 10 eyes; uveitis, 6 eyes). Twenty-nine healthy eyes of 26 subjects (11 men, 16 women) were also included for analysis. Healthy subjects ranged in age from 33 to 77 years old (mean ± SD, 62.6 ± 14.2 years), in spherical equivalent refractive errors from –6.0 to 1.5 (–1.47 ± 2.50 D), in axial length from 22.11 to 26.55 mm (mean ± SD, 24.1 ± 1.20 years). No significant differences between sex, age, and axial length were found between glaucomatous and healthy eyes ($P = 0.378$, 0.936, and 0.607, respectively).

3D Images of Lamina Cribrosa in Normal Eyes

En face sectioned volume images on SS-OCT with a 1050-nm tunable laser visualized the lamina cribrosa as a highly reflective structure with multiple less reflective dots corresponding to lamina pores (Fig. 1). The highly reflective lamina cribrosa was seen even beneath the neuroretinal rim but became hyporeflective beneath the peripapillary structures that compose the border tissue, choroid, and sclera. There were strap-like hyporeflective patterns on the highly reflective lamina cribrosa, particularly in the nasal half (Fig. 1C, yellow arrowheads). The hyporeflectivity corresponded well to the retinal blood vessels on disc photographs compared between reconstructed serial en face images (Fig. 1B) or en face volume images (Fig. 1C) to the disc photographs (Fig. 1A). In serial SS-OCT B-scans, the hyporeflective regions in the lamina cribrosa corresponding to the retinal blood vessels on en face images (Fig. 1B) showed axially straight hyporeflective bands (termed vascular shadowing) throughout the B-scan image beneath the retinal blood vessels (Fig. 1D). The retinal trunk vessels caused large hyporeflective areas in the center of the nasal half of the lamina cribrosa (Fig. 1C, arrow).

3D Images of Focal Lamina Cribrosa Defects in Glaucomatous Eyes

Some glaucomatous eyes showed hyporeflective spots in the highly reflective lamina cribrosa (Fig. 2, red arrowhead). This feature did not correspond with retinal blood vessels when the en face serial B-scan (Fig. 2B) or en face sectioned volume (Fig.

Investigative Ophthalmology & Visual Science

Downloaded From: https://iovs.arvojournals.org/pdfaccess.ashx?url=/data/journals/iovs/932985/ on 11/11/2018

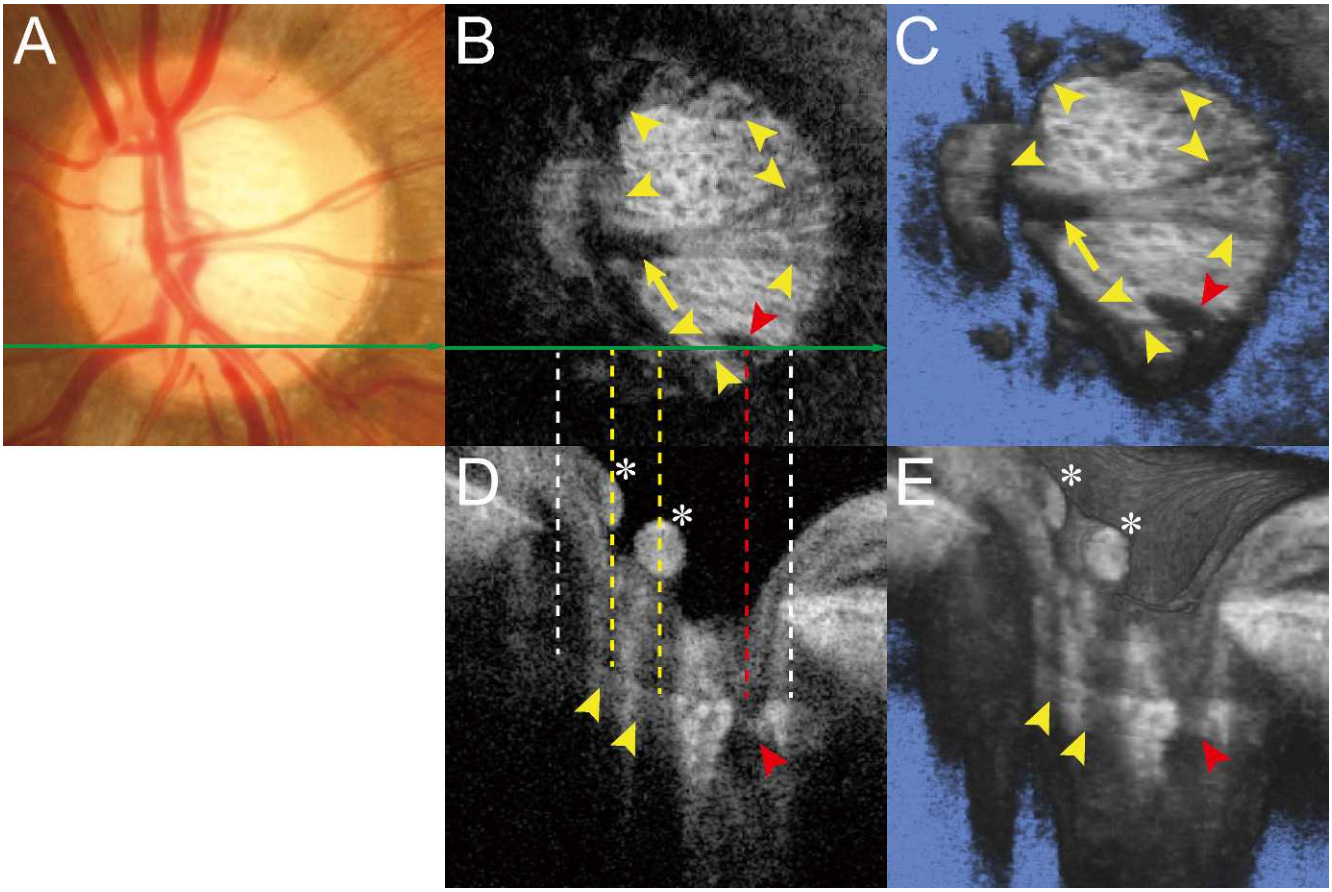

FIGURE 2. 3D imaging of the lamina cribrosa with SS-OCT at 1050 nm in a glaucomatous eye. (**A**) Color disc photograph. (**B**) En face image of the optic disc at the level of the lamina cribrosa reconstructed from a 3D SS-OCT data set. A comparison between the disc photograph and the en face image revealed that the hyporeflective pattern (*yellow arrowheads*) accurately corresponds to retinal blood vessels on the optic disc, with the exception of the inferotemporal triangle defect (*red arrowhead*). The hyporeflective features corresponding to the retinal blood vessels are artifacts that resulted from signal blocking by the retinal blood vessels (termed vascular shadowing). (**C**) En face volume image sectioned at the level of the lamina cribrosa reconstructed from the 3D SS-OCT data set. Artifactual defects (*yellow arrowheads*) of the highly reflective lamina cribrosa are caused by vascular shadowing, and the *red arrowhead* points at the focal lamina cribrosa defect. (**D, E**) Horizontal B-scan (**D**) and sectioned volume (**E**) images along the *green line* (**A**, **B**). Lamina cribrosa reflectivity appears to have defects (*arrowheads*). The defects indicated (*yellow arrowheads*) correspond to the hyporeflective vascular regions identified in ([**B**], *yellow dotted line*), thus indicating that these are artifacts resulting from the retinal blood vessels (*asterisks*) and are not lamina cribrosa defects. The defect indicated by a *red arrowhead* shows full-thickness loss of lamina reflectivity. We defined this feature as a focal lamina cribrosa defect with a lamina cavity shape. Note, the vascular shadowing shows an axially straight hyporeflectivity throughout the area beneath the blood vessels (*asterisks*), whereas the margin of the lamina cribrosa defect is not straight.

2C) images were compared to the disc photographs (Fig. 2A). The hyporeflective spots were much larger in size and much lower in reflectivity than the hyporeflective dots representing laminar pores. On serial B-scan images, this hyporeflective spot showed a full-thickness defect in the highly reflective lamina cribrosa. This feature was defined as a focal full-thickness lamina cribrosa defect. There was excellent agreement in identifying this feature between the two graders (Cohen's κ, 0.768; $P < 0.001$). The graders agreed that 19 focal lamina defects were present in 12 eyes (11 patients, 6.6%) of 182 eyes with glaucoma. In contrast, no lamina defects were found in 29 healthy eyes of 26 age-matched participants. No defects in conus structure (i.e., conus pits)[25] were found in any peripapillary regions.

The number of the focal lamina defects per eye was 1 in 6 eyes, 2 in 5 eyes, and 3 in 1 eye, with an average of 1.58 $\pm$ 0.67. Of the 19 lamina defects in 12 eyes, 4 defects of 4 eyes were located at or near the superior optic disc margin, 13 defects of 10 eyes at or near the inferior optic disc margin, and 2 defects of 2 eyes at or near the temporal optic disc margin.

Nine eyes (75.0%) showed 15 lamina defects with a round or oval shape in the vicinity of the margin of the lamina cribrosa on en face images, which appeared to be like a longitudinal cavity (Figs. 3A–D) in the lamina cribrosa on serial B-scans. We called this type of lamina defect a "lamina cavity." The remaining 3 eyes (23.1%) showed four triangular lamina defects at the margin of the lamina cribrosa (Figs. 3E–L) on en face images.

In horizontal serial B-scans, the highly reflective lamina cribrosa appeared to be detached from the sclera (Figs. 3F, 3H, 3J, 3L). We called this type of lamina defect a "lamina disinsertion." None of these eyes included both the lamina cavity and lamina disinsertion.

Seven (58.3%) of the 12 eyes with focal lamina cribrosa defects had concurrent or previous disc hemorrhages. Nine (81.8%) of 11 lamina cribrosa defects in these 7 eyes spatially corresponded with the disc hemorrhages (Fig. 4). Of 11 lamina

Investigative Ophthalmology & Visual Science

Downloaded From: https://iovs.arvojournals.org/pdfaccess.ashx?url=/data/journals/iovs/932985/ on 11/11/2018

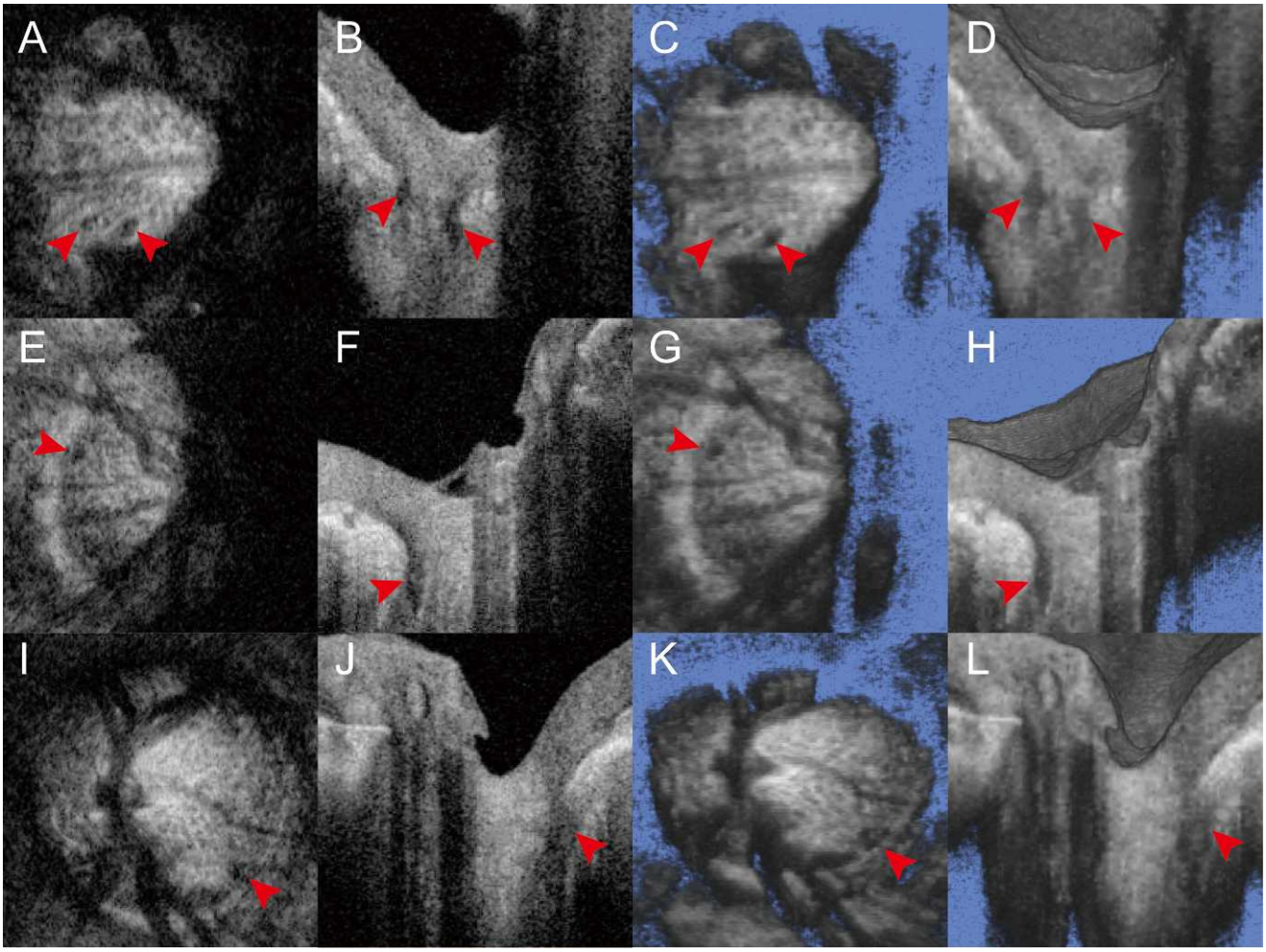

FIGURE 3. Two types of full-thickness lamina cribrosa defects. (**A–D**) Lamina cavity type; (**E–L**) lamina disinsertion type. (**A**, **E**, **I**) Single en face scan images; (**B**, **F**, **J**) single horizontal B-scan images; (**C**, **G**, **K**) en face volume image sectioned at the lamina cribrosa level; (**D**, **H**, **L**) horizontal sectioned volume images. *Red arrowheads* indicate full-thickness defects of the lamina cribrosa reflectivity.

defects, 8 and 3 defects were lamina cavity and lamina disinsertion, respectively; this difference was not statistically different ($P = 0.369$).

Of 19 lamina defects of 12 eyes, all of the lamina defects spatially corresponded with the neuroretinal rim thinning, 13 (68.4%) of 9 eyes spatially corresponded with localized RNFL defects, and 12 (68.4%) lamina cribrosa defects of the 9 eyes spatially corresponded with the abnormal circumpapillary RNFL (cpRNFL) thickness in the cpRNFL sector analysis using Spectralis (Fig. 4). Visual field defects were found in the corresponding hemifield in 13 (68.4%) of 17 lamina cribrosa defects located in the superior or inferior lamina (Fig. 4). Five eyes that showed lamina cribrosa defects limited to the inferior half of the lamina cribrosa had greater loss of sensitivity in the superior hemifield. Of 19 lamina cribrosa defects, average mean ± SD MD values were –7.41 ± 7.37 dB and –10.47 ± 7.02 dB in eyes with lamina cavities and lamina disinsertions, respectively; this difference was not statistically different ($P = 0.375$).

Acquired pits in the optic nerve were found only in 6 (3.3%) eyes. Three (50%) of the 6 eyes had concurrent or previous disc hemorrhages ($P = 0.092$). Lamina cribrosa defects were found in only 1 of the 6 eyes with APON, thus not significantly associated with APON.

Comparison Between Clinical Characteristics of Eyes With Focal Lamina Cribrosa Defects and Those Without

Clinical characteristics were compared between eyes with and those without focal full-thickness lamina defects (Table 1). No significant differences were found in sex or age between eyes with and without lamina defects. The focal lamina cribrosa defects were found in 1 of 62 eyes with HTG (1.6%), 10 (9.6%) of 104 eyes with NTG, and 1 (6.3%) of 16 eyes with secondary glaucoma. Thus, focal lamina cribrosa defects were found most frequently in eyes with NTG, but this was not statistically significant ($P = 0.132$) (Table 1).

No significant differences were found in visual field MD, disc size, cup-to-disc (C/D) ratio on HRT2, maximum untreated IOP, and cpRNFL thickness as measured with Spectralis HRA+OCT. The eyes with the lamina cribrosa defects were more myopic and had significantly longer axial lengths than those without focal lamina defects ($P = 0.029$ and $P = 0.004$, Mann-Whitney U test, respectively). Concurrent or previous occurrence of disc hemorrhage was more frequently found in eyes with the lamina defects ($P = 0.002$). In 5 eyes (71.4%), the lamina defects were spatially associated with concurrent disc hemorrhages.

Investigative Ophthalmology & Visual Science

Downloaded From: https://iovs.arvojournals.org/pdfaccess.ashx?url=/data/journals/iovs/932985/ on 11/11/2018

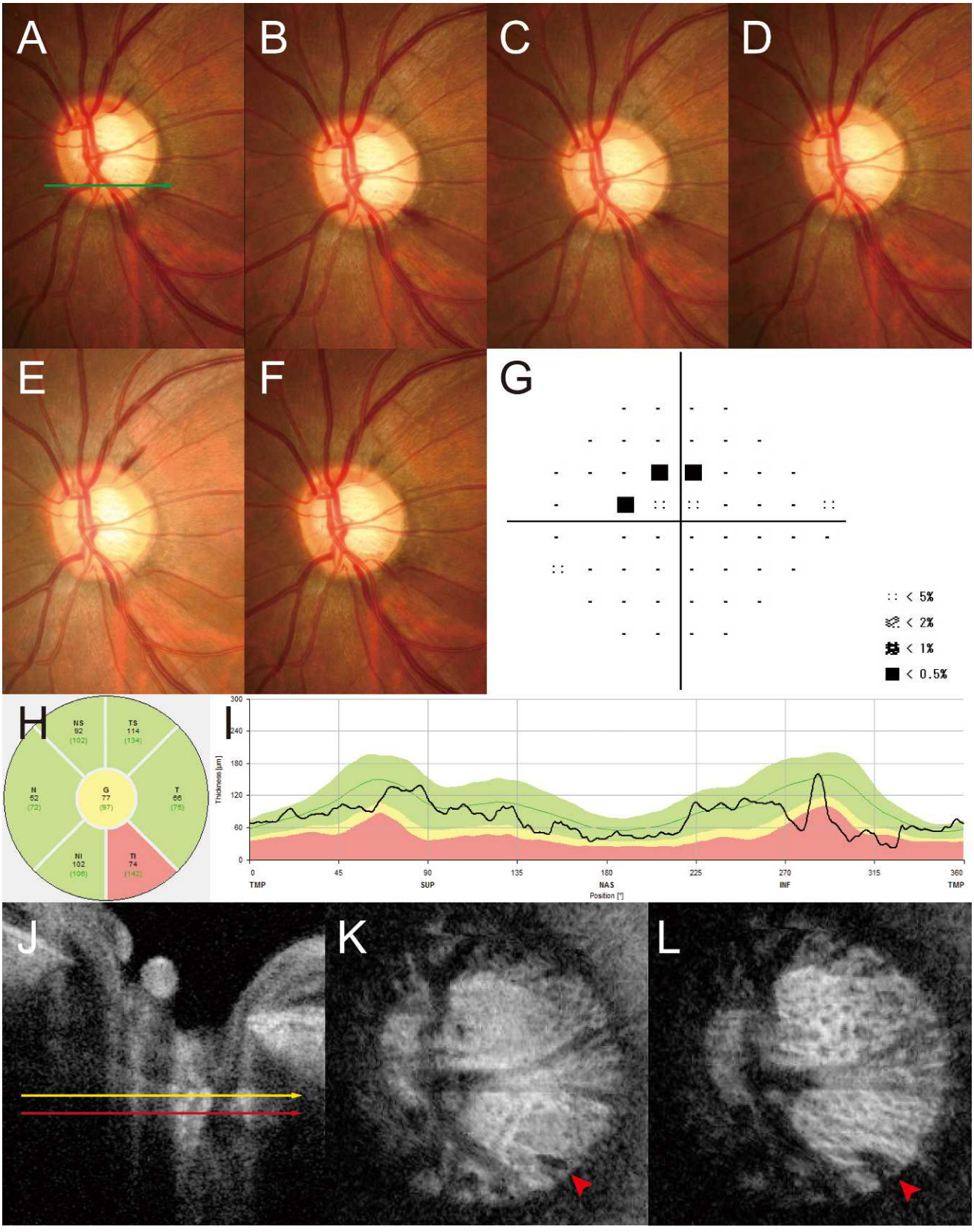

Figure 4. A case that shows the spatial correlations of a 3D-identified lamina cribrosa defect (lamina cavity) with repeated disc hemorrhages (**A**–**F**), localized RNFL defects (**A**–**F**), visual field defects (**G**), and abnormal cpRNFL thickness (**H**, **I**). The left eye of a 43-year-old woman with normal tension glaucoma who presented with repeated disc hemorrhages. Mean deviation in the visual field on static automated perimetry was −2.03 decibels; baseline intraocular pressure was 15.0 mm Hg; and axial length was 23.70 mm. (**A**–**F**) Color disc photographs. Disc hemorrhages were found at the initial visit (**A**) and at 3 (**B**), 12 (**C**), 15 (**D**), 21 (**E**), and 24 (**F**) months in similar locations associated with the inferotemporal RNFL defect and superotemporal slit-like RNFL defects. (**G**) Standard automated perimetry 24-2 pattern deviation map. Paracentral visual field defects were detected in the superior hemifield. (**H**) Classification map of regional cpRNFL thickness (**H**) and cpRNFL thickness map (**I**) on Spectralis.

Investigative Ophthalmology & Visual Science

Downloaded From: https://iovs.arvojournals.org/pdfaccess.ashx?url=/data/journals/iovs/932985/ on 11/11/2018

Abnormal cpRNFL thickness (<1%, indicated by *red*) compared to the confidence interval of a normative database was detected in the inferotemporal region. (**J**) A SS-OCT B-scan along the *green line* (**A**). (**K**, **L**) Serial en face images at different levels of lamina cribrosa depth ([**K**], *yellow line* in [**J**]; [**L**], *red line* in [**J**]) reconstructed from the 3D SS-OCT data set. A full-thickness, cavity-type lamina cribrosa defect is seen in the vicinity of the disc hemorrhage and the localized RNFL defect in the inferotemporal region. The size of the lamina cribrosa defect is larger in the deeper en face images.

The presence of lamina cribrosa defects was significantly associated with longer axial length and concurrent or previous disc hemorrhage occurrence in both univariate ($P < 0.001$ and 0.002, respectively) and multivariate ($P = 0.033$ and 0.024, respectively) logistic regression analyses (Table 2), but not with age, visual field MD, NTG, disc size, vertical C/D ratio, maximum untreated IOP, or cpRNFL thickness.

Discussion

As we previously reported, SD-OCT allowed 3D imaging of the gross structures of lamina cribrosa and pores, except for the structure beneath the neuroretinal rim.[14] EDI-OCT further improved visualization of the whole structure of the lamina cribrosa in B-scans, particularly beneath the neuroretinal rim.[17–19] The current study showed that SS-OCT at 1050 nm allowed 3D imaging of the whole lamina structures including the structure beneath the neuroretinal rim. Lamina cribrosa defects were thus found only by the EDI-OCT (in earlier studies)[20,21] and SS-OCT at 1050 nm (current study), probably because they were located at or in the vicinity of the lamina cribrosa margins beneath the neuroretinal rim. However, it remains difficult to visualize the laminar structure beneath retinal blood vessels because of signal loss due to vascular shadowing,[26] which must be taken into consideration for evaluation of hyporeflective lesions including lamina cribrosa defects (Fig. 1). On en face serial or sectioned volume images, the signal blocking appeared as a hyporeflective vascular pattern, which corresponded to retinal blood vessels on disc photographs. In the current study, we eliminated hyporeflective lesions due to vascular shadowing by comparing B-scans and en face images.

We analyzed two types of full-thickness focal lamina defects, the lamina cavity and lamina disinsertion. Kiumehr et al.[21] originally reported five categories of focal lamina cribrosa defects based on shape: smooth indentation, moth-eaten appearance defect, step-like depression, hole-like defect, and altered laminar insertion. However, the same research group included hole-like defects (laminar holes) and prominently altered laminar insertions (laminar disinsertions) to assess the association between lamina cribrosa defects and neuroretinal rim loss and APON because they aimed to avoid misclassification of normal anatomical variations and artifacts as real glaucomatous focal lamina cribrosa defects by using stricter criteria.[27] Our strategy is consistent with this approach, and the lamina cavity and lamina disinsertion on 3D SS-OCT in the current study appear to correspond to the hole-like defects and altered laminar insertions, respectively, in the earlier study. In order to interpret the findings of the earlier and present studies, it must be taken into consideration that only eyes with full-thickness lamina cribrosa defects were included for further analysis.

Kiumehr et al.[21] showed that focal lamina cribrosa defects corresponded with glaucomatous optic disc changes such as neuroretinal rim thinning/notching or an APON. Park et al. also showed a spatial correlation between focal lamina cribrosa defects and disc hemorrhages as well as neuroretinal rim loss and RNFL defects (Park SC, et al. *IOVS* 2012;53:ARVO E-Abstract 3695). In the current study, full-thickness lamina cribrosa defects spatially corresponded with neuroretinal rim thinning (100%), localized RNFL defects (68.4%), abnormal cpRNFL thickness in the cpRNFL sector analysis on Spectralis (68.4%), and disc hemorrhages (81.8%), consistent with the earlier 2 studies. Thus, lamina cribrosa defects appear to be

Table 1. Comparison of Clinical Characteristics Between Glaucomatous Eyes With and Without Focal Lamina Defects

Patient Characteristics	Lamina Cribrosa Defect		*P* Value
	Found	Not Found	
Male	5 (5)	80 (49)	0.377*
Female	7 (6)	90 (61)	
Age, y	58.3 ± 11.3 (42–75)	63.2 ± 14.6 (21–89)	0.114†
Refractive error, D	−3.19 ± 1.91 (−6 to 0)	−1.63 ± 2.20 (−6 to 3)	**0.029†**
Axial length, mm	25.8 ± 1.53 (23.7–27.9)	24.4 ± 1.20 (21.4–27.0)	**0.004†**
Mean deviation, dB	−9.96 ± 7.68 (−25.36 to −1.58)	−11.2 ± 9.3 (−31.3 to 0.63)	0.815†
Disc size, mm	2.08 ± 0.37 (1.44–2.52)	2.24 ± 0.52 (1.02–4.02)	0.270†
Vertical C/D ratio	0.41 ± 0.16 (0.09–0.56)	0.50 ± 0.20 (0.04–0.91)	0.055†
Diagnosis, no. of eyes	HTG, 1 NTG, 10 SG, 1	HTG, 61 NTG, 94 SG, 15	0.132*
NTG/total, no. of eyes	10/12	94/170	0.058*
Maximum untreated IOP, mm Hg	20.4 ± 7.95 (15–43)	21.1 ± 6.92 (8–44)	0.356†
cpRNFL thickness, μm	67.9 ± 10.9 (51–87)	69.7 ± 16.8 (33–113)	0.739†
Localized RNFL defects, no. of eyes (no. of patients)	8 (8)	77 (56)	0.152*
Disc hemorrhage, no. of eyes (no. of patients)			
Present	7 (7)	33 (27)	**0.002***
Absent	5 (4)	137 (98)	

Values are mean ± SD with ranges in parentheses. Bold indicates P < 0.05. SG, secondary glaucoma.
* χ^2 test.
† Mann-Whitney *U* test.

Investigative Ophthalmology & Visual Science

Downloaded From: https://iovs.arvojournals.org/pdfaccess.ashx?url=/data/journals/iovs/932985/ on 11/11/2018

Table 2. Univariate and Multivariate Logistic Regression Analyses for Focal Lamina Defects in Patients With Glaucoma

	Univariate		Multivariate	
Clinical Characteristics	**Beta (SE)**	***P* Value**	**Beta (SE)**	***P* Value**
Age	−0.001 (0.001)	0.253	0.002 (0.002)	0.457
Axial length	0.060 (0.016)	**<0.001***	0.062 (0.029)	**0.033**
Visual field MD	0.001 (0.002)	0.641	−0.006 (0.005)	0.267
NTG	0.071 (0.037)	0.058	0.083 (0.082)	0.313
Disc size	−0.041 (0.039)	0.293	−0.043 (0.074)	0.560
C/D ratio	−0.159 (0.099)	0.110	−0.250 (0.225)	0.269
Maximum untreated IOP	−0.001 (0.003)	0.753	0.005 (0.008)	0.525
cpRNFL thickness	−0.001 (0.001)	0.722	0.001 (0.003)	0.865
Localized RNFLD	0.053 (0.038)	0.153	−0.006 (0.065)	0.924
Disc hemorrhage	0.140 (0.043)	**0.002***	0.152 (0.066)	**0.024**

Bold indicates $P < 0.05$.

well associated with clinical manifestations that present with localized glaucomatous damages.

In our multivariate logistic regression analyses, lamina cribrosa defects were significantly associated with concurrent or previous disc hemorrhages. Hsu et al. found that the mean follow-up IOP, disc hemorrhage detection, and visual field MD were associated with focal lamina cribrosa defects in multivariate logistic regression analysis (Hsu AT, et al. *IOVS* 2012;53:ARVO E-Abstract 2815). Thus, our results agreed with those of the earlier study regarding disc hemorrhage detection. Disc hemorrhages are thought to be related to localized glaucomatous damages because they have often been associated with rim notching and localized RNFL defects and focal glaucoma progression.[28–32] Local disruption of lamina beams or laminar pore structures may not only cause RGC axon damages but also lead to rupture of prelaminar or laminar beam capillaries, and subsequently may lead to the concurrent focal glaucoma progression and disc hemorrhages, although this remains speculative.

Our results did not agree for IOP and visual field MD. However, because the frequency of full-thickness lamina cribrosa defects was small in the current study, the number of eyes with this feature was only 13. Thus, we cannot be certain that the factors that were found to be statistically insignificant in this study, such as demographics, disc size, maximum untreated IOP, visual field MD, or RNFL thickness, are definitely not associated with the presence of lamina cribrosa defects.

In contrast, the correspondence between lamina cribrosa defects and APON seemed to be much lower. APON has been described as a unique feature on disc photography showing a deep, localized excavation of the neuroretinal rim with sharply localized depression and loss of normal laminar architecture of the lamina cribrosa. The prevalence of APON in glaucomatous eyes was 2.8% to 6.6%.[33–36] In the current study, the prevalence of APON was 3.3%, almost consistent with these earlier studies. It was uncertain whether lamina cribrosa defects and APON are identical, different, or overlapped. The APON was reportedly more frequently located inferiorly[34–36] and was associated with visual field defects,[33–36] visual field progression,[34] and disc hemorrhages.[34,36] Thus, focal lamina cribrosa defects and APON appear to have similar clinical characteristics. However, in the current study, focal lamina cribrosa defects were a little more prevalent (6.6%) and found only in 1 of the 6 eyes with APON. It is possible that some of these 5 eyes with APON, but without laminar defects, had defective changes limited to the prelaminar tissue, or the surface of the lamina cribrosa. Otherwise, it is also possible that structural changes in the lamina cribrosa associated with APON appearance was unable to be detected due to the limitation of our imaging method. Furthermore, Kiumehr et al.[21] showed that only 11 (16.2%) eyes of 68 full-thickness lamina cribrosa defects (5 [50.0%] of 10 hole-like defects, and 6 [10.3%] of 58 altered laminar insertions) presented clinically as an APON. In the current study, only 8 (40.0%) of the 20 eyes with full-thickness lamina cribrosa defects showed an associated APON. Thus, only a part of full-thickness lamina cribrosa defects appears to present clinically as an APON. It is possible that detection of these focal lamina cribrosa defects is difficult on the disc photography, because it is a structural abnormality present beneath the prelaminar tissue and sometimes beneath the neuroretinal rim. Furthermore, some lamina cribrosa defects became larger at the greater depth where disc photographs cannot visualize the structure clearly.

In multivariate logistic regression analyses, the lamina cribrosa defects were also associated with longer axial length. Recently, Ohno-Matsui et al.,[25] using the same SS-OCT system as ours, reported that pit-like clefts in the optic disc (termed acquired optic disc pits) and myopic conus (conus pits) were found in 16.2% of in eyes with pathologic myopia with extreme myopia (inclusion criteria, spherical equivalent refractive errors > -8.00 diopters or axial length > 26.5 mm; included mean refractive error, -14.5 ± 4.3 diopter, and mean axial length, 30.0 ± 2.1 mm). The shape of the lamina cribrosa defects in our glaucomatous subjects appear to be, at least in part, identical to that of the optic disc pits in the pathologic myopia, particularly in the characteristics that both features were full-thickness defects of the lamina cribrosa. In the current study, to exclude the influence of pathologic myopia, we excluded eyes with extreme high myopia. Different from the findings in the eyes with extreme myopia, we found no conus pits outside the optic disc, or no discontinuous nerve fiber layer overlying the optic disc pits.[25] Furthermore, optic disc pits in the pathologic myopia were more deeply excavated than the lamina cribrosa defects in our glaucomatous eyes. Regardless of these differences, the prevalence of the "acquired optic disc pits" in pathologic myopia was 5.6%, comparable with that of lamina cribrosa defects (6.6%) in the current study. Furthermore, the eyes with optic disc pits in the extreme high myopia were also significantly more myopic and had significantly longer axial lengths than the highly myopic eyes without any kind of pits in the optic disc area, consistent with our results. Although it is uncertain whether the "optic disc pits" in pathologic myopia and lamina cribrosa defects in our glaucomatous eyes are different, identical, or overlapped, mechanical stress to lamina cribrosa via peripapillary scleral deformation according to axial length elongation may be a common pathway involved in the development of these defective changes of lamina cribrosa.

Investigative Ophthalmology & Visual Science

Downloaded From: https://iovs.arvojournals.org/pdfaccess.ashx?url=/data/journals/iovs/932985/ on 11/11/2018

Most of the full-thickness lamina cribrosa defects were located at or near the superior optic disc margin, consistent with earlier studies.[21,27] Histopathological studies revealed the following regional variations of the lamina cribrosa in presumably healthy human eyes: the superior and inferior portions, compared to the nasal and temporal regions, had larger single pore areas and summed pore areas, thinner connective tissue, and less glial cell support.[37–39] These regional variations, which are thought to account for the greater susceptibility to early glaucomatous damage in the superior and inferior portions, may be responsible for the frequent detection of full-thickness lamina cribrosa defects in these susceptible locations.

Gross deformation of lamina cribrosa, such as thinning, posterior displacement, and excavation beneath the anterior scleral canal, has been thought to damage the RGC axons. The laminar gross deformation is thought to be caused by two types of mechanical stress generated by IOP/translaminar pressure gradient and stretching force from peripapillary sclera.[9–11] It is thought that IOP-induced deformation of the lamina cribrosa includes two components acting simultaneously in response to acute IOP elevation: one component is the effect of IOP on the anterior laminar surface, which deforms the lamina posteriorly; and the other component is the effects of IOP on the sclera, which causes an expansion of the scleral canal.[10] The effects of IOP on the sclera are transmitted to the lamina cribrosa through its insertion into the canal wall, generating a tensile stretch that causes the lamina to pull "taut," thereby causing anterior displacement. Thus, acute tensile stretch imposed on the lamina can be generated by the expanding scleral canal after acute IOP rise. Continuous tensile stretch may also be yielded by translaminar pressure gradient. The magnitude and distribution of the strains on the lamina cribrosa from the tensile stretch depend on the assumed regional variation of mechanical properties of the lamina cribrosa and sclera. The superior and inferior parts of the lamina cribrosa contain larger pores and thinner connective tissue than other parts.[37–39] All models of laminar biomechanics consistently predict regions of relatively large strain in the peripheral lamina.[10] It is interesting that a large part of lamina cribrosa defects were found in the peripheral lamina in the inferior and superior parts that would suffer from the relatively large tensile stress. Disc hemorrhages are also frequently found in this location. We speculate that tensile stretch generates large strain in a local region of the peripheral lamina in the inferior or superior parts, and subsequently leads to mechanical disruption of lamina cribrosa, particularly resulting in lamina disinsertion. Myopic thinning of the lamina cribrosa may cause the susceptibility of the lamina cribrosa to mechanical disruption.[40] Furthermore, mechanical expansion of scleral canal as a result of myopic peripapillary scleral deformation according to axial length elongation may enhance tensile stretch or cause uneven tensile stretch. The association of lamina cribrosa defects with longer axial length favors these speculations.

This study includes some limitations. One limitation is the poor visualization of the nasal half of the lamina cribrosa on en face SS-OCT images. In glaucoma, retinal trunk vessels are often shifted to the nasal half of the optic disc, and consequently prominent shadowing effects by assembling large retinal vessels cause poor visualization of the nasal part of the lamina cribrosa. We cannot deny the possibility that focal lamina cribrosa defects were present also in the nasal portion. The second limitation is that our study subjects were all Japanese. Probably because of this, 57.1% of the study eyes had NTG. Such a high percentage of NTG patients would affect the relationship between the lamina cribrosa defects and clinical factors. This should be taken into consideration to interpret our results. However, in the current study, although lamina cribrosa defects were more frequently found in eyes with NTG than without NTG, NTG was not a significant risk factor for lamina cribrosa defects in multivariate analysis. Third limitation is that the current study is a cross-sectional study. Therefore, it remains uncertain whether the lamina cribrosa defects on 3D SS-OCT imaging is permanent, progressive, or transient (i.e., reversible). It is possible that the lamina cribrosa defects are more prevalent when observed in longitudinal studies.

Conclusions

In conclusion, the current study showed that 3D SS-OCT imaging is a useful method for detection of focal full-thickness lamina cribrosa defects because it can differentiate between actual lamina cribrosa defects and artifacts due to vascular shadowing. Disc hemorrhages and longer axial length were risk factors for the presence of lamina cribrosa defects. Disc hemorrhages are known to be associated with local glaucoma progression, as well as localized RNFL damages.[28–32] These findings raise the question whether the lamina cribrosa defects are related to local glaucoma progression. Further studies in longitudinal basis are needed to clarify this question in the future.

Acknowledgments

Disclosure: **K. Takayama**, None; **M. Hangai**, Nidek (F, S), Topcon (F, C), Heidelberg Engineering (R), Santen (R), Topcon (F), Canon (F); **Y. Kimura**, None; **S. Morooka**, None; **M. Nukada**, None; **T. Akagi**, None; **H.O. Ikeda**, None; **A. Matsumoto**, Topcon (E); **N. Yoshimura**, Nidek (F, R, S), Topcon (F, R), Canon (F, R)

References

1. Minckler DS, Bunt AH, Johanson GW. Orthograde and retrograde axoplasmic transport during acute ocular hypertension in the monkey. *Invest Ophthalmol Vis Sci*. 1977;16:426–441.
2. Quigley HA, Addicks EM, Green WR, Maumenee AE. Optic nerve damage in human glaucoma. II. The site of injury and susceptibility to damage. *Arch Ophthalmol*. 1981;99:635–649.
3. Quigley HA, Hohman RM, Addicks EM, Massof RW, Green WR. Morphologic changes in the lamina cribrosa correlated with neural loss in open-angle glaucoma. *Am J Ophthalmol*. 1983;95:673–691.
4. Ogden TE, Duggan J, Danley K, Wilcox M, Minckler DS. Morphometry of nerve fiber bundle pores in the optic nerve head of the human. *Exp Eye Res*. 1988;46:559–568.
5. Bellezza AJ, Rintalan CJ, Thompson HW, Downs JC, Hart RT, Burgoyne CF. Deformation of the lamina cribrosa and anterior scleral canal wall in early experimental glaucoma. *Invest Ophthalmol Vis Sci*. 2003;44:623–637.
6. Anderson DR. Ultrastructure of human and monkey lamina cribrosa and optic nerve head. *Arch Ophthalmol*. 1969;82:800–814.
7. Emery JM, Landis D, Paton D, Boniuk M, Craig JM. The lamina cribrosa in normal and glaucomatous human eyes. *Trans Am Acad Ophthalmol Otolaryngol*. 1974;78:OP290–OP297.
8. Wilczek M. The lamina cribrosa and its nature. *Br J Ophthalmol*. 1947;31:551–565.
9. Burgoyne CF, Downs JC, Bellezza AJ, Suh JK, Hart RT. The optic nerve head as a biomechanical structure: a new paradigm for understanding the role of IOP-related stress and strain in the pathophysiology of glaucomatous optic nerve head damage. *Prog Retin Eye Res*. 2005;24:39–73.

Downloaded From: https://iovs.arvojournals.org/pdfaccess.ashx?url=/data/journals/iovs/932985/ on 11/11/2018

10. Crawford Downs J, Roberts MD, Sigal IA. Glaucomatous cupping of the lamina cribrosa: a review of the evidence for active progressive remodeling as a mechanism. *Exp Eye Res*. 2011;93:133–140.
11. Burgoyne CF. A biomechanical paradigm for axonal insult within the optic nerve head in aging and glaucoma. *Exp Eye Res*. 2011;93:120–132.
12. Ren R, Jonas JB, Tian G, et al. Cerebrospinal fluid pressure in glaucoma: a prospective study. *Ophthalmology*. 2010;117: 259–266.
13. Kagemann L, Ishikawa H, Wollstein G, et al. Ultrahigh-resolution spectral domain optical coherence tomography imaging of the lamina cribrosa. *Ophthalmic Surg Lasers Imaging*. 2008;39:S126–S131.
14. Inoue R, Hangai M, Kotera Y, et al. Three-dimensional high-speed optical coherence tomography imaging of lamina cribrosa in glaucoma. *Ophthalmology*. 2009;116:214–222.
15. Strouthidis NG, Grimm J, Williams GA, Cull GA, Wilson DJ, Burgoyne CF. A comparison of optic nerve head morphology viewed by spectral domain optical coherence tomography and by serial histology. *Invest Ophthalmol Vis Sci*. 2010;51:1464–1474.
16. Agoumi Y, Sharpe GP, Hutchison DM, Nicolela MT, Artes PH, Chauhan BC. Laminar and prelaminar tissue displacement during intraocular pressure elevation in glaucoma patients and healthy controls. *Ophthalmology*. 2011;118:52–59.
17. Lee EJ, Kim TW, Weinreb RN, Park KH, Kim SH, Kim DM. Visualization of the lamina cribrosa using enhanced depth imaging spectral-domain optical coherence tomography. *Am J Ophthalmol*. 2011;152:87–95.e81.
18. Park HY, Jeon SH, Park CK. Enhanced depth imaging detects lamina cribrosa thickness differences in normal tension glaucoma and primary open-angle glaucoma. *Ophthalmology*. 2012;119:10–20.
19. Lee EJ, Kim TW, Weinreb RN, et al. Three-dimensional evaluation of the lamina cribrosa using spectral-domain optical coherence tomography in glaucoma. *Invest Ophthalmol Vis Sci*. 2012;53:198–204.
20. Park SC, De Moraes CG, Teng CC, Tello C, Liebmann JM, Ritch R. Enhanced depth imaging optical coherence tomography of deep optic nerve complex structures in glaucoma. *Ophthalmology*. 2012;119:3–9.
21. Kiumehr S, Park SC, Dorairaj S, et al. In vivo evaluation of focal lamina cribrosa defects in glaucoma. *Arch Ophthalmol*. 2012; 130:552–559.
22. Srinivasan VJ, Adler DC, Chen Y, et al. Ultrahigh-speed optical coherence tomography for three-dimensional and en face imaging of the retina and optic nerve head. *Invest Ophthalmol Vis Sci*. 2008;49:5103–5110.
23. Hirata M, Tsujikawa A, Matsumoto A, et al. Macular choroidal thickness and volume in normal subjects measured by swept-source optical coherence tomography. *Invest Ophthalmol Vis Sci*. 2011;52:4971–4978.
24. Jirarattanasopa P, Ooto S, Tsujikawa A, et al. Assessment of macular choroidal thickness by optical coherence tomography and angiographic changes in central serous chorioretinopathy. *Ophthalmology*. 2012;119:1666–1678.
25. Ohno-Matsui K, Akiba M, Moriyama M, et al. Acquired optic nerve and peripapillary pits in pathologic myopia. *Ophthalmology*. 2012;119:1685–1692.
26. Girard MJ, Strouthidis NG, Ethier CR, Mari JM. Shadow removal and contrast enhancement in optical coherence tomography images of the human optic nerve head. *Invest Ophthalmol Vis Sci*. 2011;52:7738–7748.
27. You JY, Park SC, Su D, Teng CC, Liebmann JM, Ritch R. Focal lamina cribrosa defects associated with glaucomatous rim thinning and acquired pits. *JAMA Ophthalmol*. 2013;131:314–320.
28. Shihab ZM, Lee PF, Hay P. The significance of disc hemorrhage in open-angle glaucoma. *Ophthalmology*. 1982;89:211–213.
29. Jonas JB, Xu L. Optic disk hemorrhages in glaucoma. *Am J Ophthalmol*. 1994;118:1–8.
30. Sugiyama K, Tomita G, Kitazawa Y, Onda E, Shinohara H, Park KH. The associations of optic disc hemorrhage with retinal nerve fiber layer defect and peripapillary atrophy in normal-tension glaucoma. *Ophthalmology*. 1997;104:1926–1933.
31. Sugiyama K, Uchida H, Tomita G, Sato Y, Iwase A, Kitazawa Y. Localized wedge-shaped defects of retinal nerve fiber layer and disc hemorrhage in glaucoma. *Ophthalmology*. 1999;106: 1762–1767.
32. De Moraes CG, Prata TS, Liebmann CA, Tello C, Ritch R, Liebmann JM. Spatially consistent, localized visual field loss before and after disc hemorrhage. *Invest Ophthalmol Vis Sci*. 2009;50:4727–4733.
33. Radius RL, Maumenee AE, Green WR. Pit-like changes of the optic nerve head in open-angle glaucoma. *Br J Ophthalmol*. 1978;62:389–393.
34. Ugurlu S, Weitzman M, Nduaguba C, Caprioli J. Acquired pit of the optic nerve: a risk factor for progression of glaucoma. *Am J Ophthalmol*. 1998;125:457–464.
35. Nduaguba C, Ugurlu S, Caprioli J. Acquired pits of the optic nerve in glaucoma: prevalence and associated visual field loss. *Acta Ophthalmol Scand*. 1998;76:273–277.
36. Healey PR, Mitchell P. The prevalence of optic disc pits and their relationship to glaucoma. *J Glaucoma*. 2008;17:11–14.
37. Quigley HA, Addicks EM. Regional differences in the structure of the lamina cribrosa and their relation to glaucomatous optic nerve damage. *Arch Ophthalmol*. 1981;99:137–143.
38. Radius RL, Gonzales M. Anatomy of the lamina cribrosa in human eyes. *Arch Ophthalmol*. 1981;99:2159–2162.
39. Jonas JB, Mardin CY, Schlotzer-Schrehardt U, Naumann GO. Morphometry of the human lamina cribrosa surface. *Invest Ophthalmol Vis Sci*. 1991;32:401–405.
40. Jonas JB, Berenshtein E, Holbach L. Lamina cribrosa thickness and spatial relationships between intraocular space and cerebrospinal fluid space in highly myopic eyes. *Invest Ophthalmol Vis Sci*. 2004;45:2660–2665.

Investigative Ophthalmology & Visual Science

Downloaded From: https://iovs.arvojournals.org/pdfaccess.ashx?url=/data/journals/iovs/932985/ on 11/11/2018